

Using AI and Polarized Imaging to Assist Physicians with Early Skin Cancer Diagnosis

Introduction

Skin cancer is the most common type of cancer worldwide, and more than two people die from skin cancer every hour (Rogers, Weinstock, Feldman, and Coldiron, 2015). Melanoma is the deadliest type of skin cancer and is the leading cause of 83% of skin cancer-related deaths (Tannous, Al-Arashi, Shah, and Yaroslavsky, 2009). In order to increase the chances of successful treatment, it is paramount that efforts are made by a physician to accurately diagnose melanoma and other skin-related cancers in a patient before they metastasize (Apalla, Nashan, Weller, and Castellsagué, 2017).

Artificial intelligence models are currently under development to detect melanoma and other skin cancers in their early stages, and the most cutting-edge algorithms can classify validated datasets at ~95 percent accuracy (European Society for Medical Oncology, 2018). However, this is only the case if the data is captured under optimal circumstances for maximal clarity (American Academy of Dermatology, 2019); it would be difficult for classifiers to correctly identify unclear images of skin lesions, regardless of how accurate the model is in practice (Freeman et al. 2020). In addition, since near-dermatologist-level classifiers are trained using clinical datasets to recognize skin lesions from dermoscopies (Esteva *et al.* 2017), one would need to take a picture of their own skin lesion using dermoscopic imaging techniques to obtain the best result from the classifier.

One such imaging technique, known as polarized dermoscopy, uses a polarized light source and magnifying optic, decreasing glare while also increasing the visibility of structures in the deep dermis (Louie *et al.* 2018). The light emitted from the source is first polarized linearly by a filter. When this light contacts the skin, a portion of it is reflected by the *stratum corneum* (the outermost layer of the epidermis), but the remaining light penetrates through and illuminates deeper layers of the dermis. In a process known as *randomization of polarization* (Dimitriou, Scope, Braun, Reiter, and Marghoob, 2019), a portion of the light is then backscattered in a perpendicular orientation. The backscattered light is subsequently allowed to pass through a polarizing filter in front of the optic, which has been positioned orthogonally to the light source's own polarizing filter. The filter blocks out the light reflected by the *stratum corneum*, but allows light reflected by the deeper layers to enter the optic for viewing, due to its polarization (Pan *et al.* 2008). The filtering of light reflected from the *stratum corneum* reduces glare, and allows the optic to view up to 1 millimetre below the *stratum corneum*, revealing the underlying pigmented structures and blood vessels (Rosendahl and Marozava, 2019). Some polarizing-specific skin structures also become more apparent with polarization, such as white spots that appear in basal cell carcinoma (Rosendahl and Marozava, 2019), as well as white lines, which may hint at the presence of melanoma or dermatofibroma (Cohen, Elpern, Wolpowitz, and Rosendahl, 2014). Without the use of polarization, these structures are not visible. Another advantage to using polarized dermoscopy over non-polarized dermoscopy is that polarized dermoscopy does not require direct contact with an immersion fluid on the skin to get a clearer image (Rosendahl and Marozava, 2019).

There were two purposes of this project: the first was to create a system that would assist physicians in accurately diagnosing skin lesions. The system consisted of an artificial intelligence model that classifies skin lesions, a custom polarizing light biomedical device, and a web application interface. The artificial intelligence model was trained using the publicly available Harvard *HAM10000* (*Human Against Machine with 10000 training images*) clinical dermoscopic dataset. Included in the *HAM10000* is an image set known as the Australian Rosendahl image set,

which uses pictures of skin lesions, many of which have been obtained by polarized dermoscopy methods (Tschandl, Rosendahl, and Kittler 2018). After the model was created, it was integrated into the web application interface, which allowed it to be accessible from a smartphone web browser. A custom polarizing light biomedical device (from here on referred to as the *Polarizer Device*) was created, designed to be attachable to a smartphone. Its function was to grant the smartphone's camera polarized-imaging capabilities for capturing skin lesions, in order to emulate non-contact, polarized dermoscopy techniques. As a tool for physicians to use, the artificial intelligence algorithm could be configured to upload its diagnoses of skin lesions into the physician's electronic medical record of choice, such as the McMaster *OSCAR Electronic Medical Record* (a popular open-source electronic medical record used by thousands of doctors across Canada). These products in the system were designed to be used in tandem with each other: a physician would be able to use their smartphone with the *Polarizer Device* to capture polarized light images of a patient's skin lesion, and through the web application be able to easily upload the image to the artificial intelligence model, which analyzes the lesion and provides its own diagnosis. Then the physician may use the algorithm to pass the image and analysis results directly into the patient's file on the physician's electronic medical record.

The second purpose was to investigate whether or not the accuracy of the artificial intelligence model was improved when classifying images captured by the smartphone with the *Polarizer Device* as opposed to regular, non-polarized images taken without the device's filters. As the artificial intelligence model was trained using dermoscopy images, including polarized images, it was expected that it would classify pictures taken using polarized imaging techniques more accurately than non-polarized skin lesions.

This innovation may become the impetus for a real-world product for use in a primary care setting, so that physicians are provided with a "second opinion" from this safe and easy-to-use system, reducing the chances of misdiagnosis when assessing a skin lesion. This will potentially save many patients' lives, as skin cancers are best treated when diagnosed early (Canadian Cancer Society, n.d.).

Hypothesis

It is hypothesized that by using polarized imaging to take pictures of skin lesions, the performance of the artificial intelligence classifier will improve significantly. As the model has been trained to primarily recognize dermoscopic images (including polarized images) due to being trained using the *HAM10000* dataset, it is expected that it would have more confidence in the correct diagnosis when classifying images that have been captured using the smartphone with the *Polarizer Device*.

Materials

- Linux computer
- Linearly polarizing filter sheet
- 3D printed parts
- Hot glue & hot glue gun
- Electrical tape
- DC-DC 3V voltage regulator
- Battery tray
- 4 AA batteries
- Battery connector
- Speaker wire
- 2 position electrical switch
- Soldering iron
- Magnet
- Smartphone
- White LED light

Procedure

Part 1: Creating the Polarizer Device

A 3-D printed polarizing light biomedical device has been built for a smartphone (Google Pixel 3A). The device, which is magnetically attached to a smartphone, is composed of an LED light source, and has two intermediary linearly polarizing filters, positioned perpendicular to each other (*Figure 4*). One of the filters fits in front of the smartphone's camera, while the other fits in front of the light source. The light source was created using a white LED light from a night light, wired in series to an on and off switch, four AA batteries, and a voltage regulator that kept the voltage at 2.96V DC. The light source and camera filter are adjustable via a sliding dovetail rail to be compatible with different smartphones. The filters are also easily removable.

Part 2: Artificial Intelligence Model and Interface

A machine learning classifier has been developed by the experimenter, using the artificial intelligence open-source software library, Google TensorFlow, and trained with data from the aforementioned Harvard *HAM10000* skin lesion dataset. The artificial intelligence model uses the Adam Optimization Algorithm (Kingma and Ba, 2014). A Python program was written to read the model and was implemented into a web application. The web application has been written using an HTML frontend, and an image upload program was created using PHP. This web-based infrastructure allows a user to easily upload pictures from a web browser, such as a browser on a smartphone. The web application is able to securely pass a picture to the artificial intelligence model for analysis and display the results of the model's diagnosis. The hardware used for all of the infrastructure is an Intel i5 hex-core PC running Ubuntu Linux.

Part 3: Data Collection

A qualified physician used a Google Pixel 3A smartphone with the *Polarizer Device* to capture images of consenting participants' skin lesions at his clinic, both with and without light polarization. The images were taken in a dark room; the light from the *Polarizer Device* was the only source of light. All pictures taken of skin lesions were anonymized; they had no identifiable information attached to them such as names, phone numbers or patient chart numbers, and no identifiable features such as faces or tattoos, etc. Each picture was rotated in 4 orientations and fed into the model for analysis, and diagnoses for the skin lesions were provided by a dermatologist, pathologist, and family physician.

Part 4: Web Application Interface Test and Device Effectiveness

The final part of the procedure was meant for testing the web application interface and evaluating the effectiveness of these biomedical devices. The artificial intelligence model was configured to upload the results of the data analysis to a demo *OSCAR Electronic Medical Record* system. To observe if this configuration is functional, fake patient files were created, with false patient chart numbers and other information. To protect the privacy of participants, no images from participants were used to test the web application interface. Miscellaneous images of skin conditions found on the public domain were used and uploaded to the patient's file. A Bash script was written to detect and upload these images from the patient's file to the artificial intelligence model, which returned a text file of the model's analysis of the image.

Results

57 skin lesions were captured. There were 12 benign keratoses, 5 dermatofibromas, 37 melanocytic nevi, and 3 vascular skin lesions. Each image was rotated in 4 different orientations, creating 228 images in total. During the data collection period, there were no instances of melanoma, basal cell carcinoma, or actinic keratosis. The AI returned a confidence level of the correct diagnosis, and these levels were recorded for each polarized and non-polarized image and compared with each other. The mean, standard deviation, and signal-to-noise ratio of the

confidence levels for each diagnosis were calculated and put into a table (*Figure 1*). All of the confidence levels of the correct diagnoses for both polarized and non-polarized images for each lesion were displayed in area graphs for comparison (*Figure 2*). Another set of graphs was made to map the difference in confidence between the polarized and non-polarized images (*Figure 3*). A positive value signifies a higher confidence in polarized images, while a negative value signifies a higher confidence value in non-polarized images.

When comparing the means, benign keratosis and dermatofibroma had a higher confidence when non-polarized, while melanocytic nevi and vascular skin lesions had a higher confidence when polarized. However, in most cases, the signal to noise ratio was very low, meaning that the deviation was very high compared to the mean. Polarized images had higher confidence than non-polarized images in 50.0% of benign keratosis, 65.0% of dermatofibroma, 68.2% of melanocytic nevi, and 91.7% of vascular skin lesions. Overall, in both polarized and non-polarized images, the model was most confident when classifying melanocytic nevi, and much less confident with the other three types of lesions.

Since the algorithm analyzed and passed image results successfully, it was also concluded that the interface worked as intended for a real-world application. As a product, the family physician found these biomedical devices helpful in his office, as the *Polarizer Device* was able to reveal subsurface visualized structures in a patient's lesion. The artificial intelligence interface also provided a useful second opinion on the diagnosis of a lesion.

Conclusion

The experimenter's hypothesis was partially supported. It was shown that in dermatofibroma, melanocytic nevi, and vascular skin lesions, there were more instances of higher confidence levels in polarized images than non-polarized images (*Figure 1*). Benign keratosis had the same number of lesions that had a higher confidence in polarized images as the number of lesions that had a higher confidence in non-polarized images (*Figure 1*). When analyzing the mean values, the polarized confidences were higher than non-polarized confidences with melanocytic nevi and vascular lesions, while non-polarized confidences were higher than polarized confidences with dermatofibroma and benign keratosis. However, the low signal to noise ratio in all four categories of lesions revealed that the deviations of data were too large to accurately compare mean values (*Figure 1*).

There are some possible explanations as to why some individual lesions had higher confidence in non-polarized images than polarized images: One reason could be that during the artificial intelligence model's analysis, images were reduced in resolution and converted to grayscale, rendering the visual differences between a polarized and non-polarized image trivial when analyzed by the model. The model also has not been trained completely with polarized images; some images in the HAM10000 dataset were obtained using non-polarized contact dermoscopy. Another reason may be due to the limited data in the experiment. There was only a total of 57 lesions, most of which were benign keratosis and melanocytic nevi, with only a few being dermatofibroma and vascular lesions. Other types of lesions, such as melanoma, basal cell carcinoma, and actinic keratosis, were not present in the data since there were no instances of these lesions in any of the patients during data collection. With more data, there may be a clearer correlation between polarization and confidence levels. When it comes to the data collection itself, there are some variables that are hard to control. It is difficult for a physician to take both a polarized and non-polarized image of a lesion under the exact same circumstances. For example, the lesion in the polarized image may not be as centered in the image as the non-polarized image. Both images can be digitally cropped to have the lesions in a similar location in the image, but sometimes this would compromise image resolution, and human error may cause a discrepancy

between the positions of the two images. Additionally, the *Polarizer Device* made some of the lesions' features less recognizable. With some lesions, the polarization revealed deeper visualized structures (*Figure 4*). However, with other lesions, typically benign keratosis, dermatofibroma, and vascular lesions, the polarization blurred the lesion's borders and diminished its perceived elevation, both important factors when diagnosing a skin lesion. For this reason, when it comes to human analysis, both polarized and non-polarized images may be necessary to formulate a more accurate diagnosis, as one image may reveal a feature of the lesion that the other image does not. Thus, it may still be helpful to include the use of the *Polarizer Device* and artificial intelligence web interface in a primary-care environment.

With that in mind, it is also important to remember that the artificial intelligence model is only a tool meant to assist a physician, and not to replace a pathologist or dermatologist; the diagnosis from a family physician, pathologist, or dermatologist should always supersede the artificial intelligence model's classification of a lesion. Furthermore, during an examination, a physician will ask for detailed history from a patient, such as changes in a lesion's symmetry, border, colour, or diameter, which are important factors when formulating a diagnosis. This is information that this artificial intelligence model does not have access to. If there is a discrepancy between any two diagnoses between the artificial intelligence model and a professional, the physician may wish to re-evaluate the lesion again.

Figures

Diagnosis	# of Lesions	Total	Instances with higher polarized confidence than non-polarized confidence		Non-Polarized			Polarized		
			# of Lesions	% of Lesions	\bar{x}	σ_x	SNR	\bar{x}	σ_x	SNR
Benign keratosis	12	48	24	50.0%	0.15	0.2	0.715	0.1	0.1	0.984
Dermatofibroma	5	20	13	65.0%	0.01	0.02	0.552	0.009	0.008	1.20
Melanocytic nevi	37	148	101	68.2%	0.7	0.2	3.20	0.8	0.2	4.53
Vascular lesion	3	12	11	91.7%	0.3	0.4	0.72	0.6	0.5	1.38

Figure 1. The table of the results with the four different lesion types. It was found that in dermatofibroma, melanocytic nevi, and vascular lesions, there were more instances with higher polarized confidence than non-polarized confidence, although the amount is most significant with vascular skin lesions. Benign keratosis had an equal amount of lesions that had higher polarized confidence as lesions that had higher non-polarized confidence. \bar{x} indicates the mean confidence values of the lesions, and σ_x indicates the standard deviation of the data of the lesions, and SNR indicates the signal to noise ratio, calculated by \bar{x}/σ_x . Typically, a lower SNR indicates that the deviation is high compared to the mean.

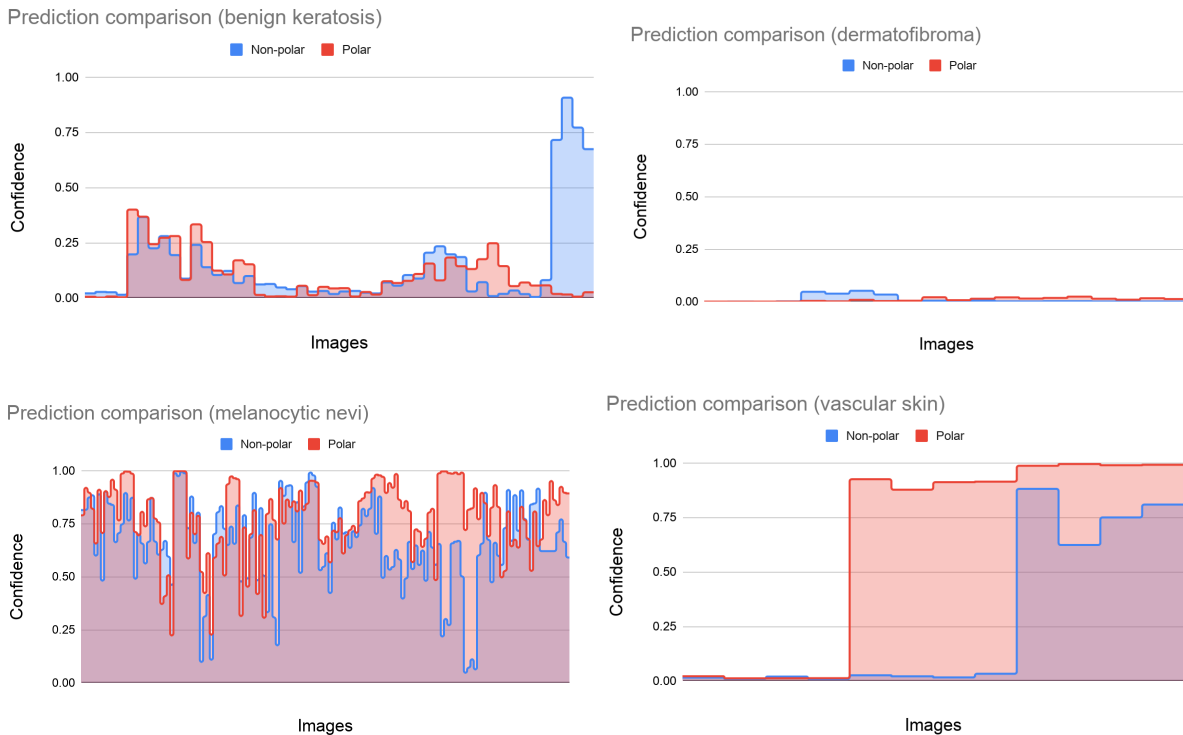


Figure 2. The confidence levels for polarized and non-polarized images for individual lesions were mapped in four area graphs, each graph for the four types of lesions. Blue bars represent the confidence of non-polarized images, while red bars indicate the confidence of polarized images. Bars that line up vertically are the corresponding polarized/non-polarized confidences of the same individual lesion.

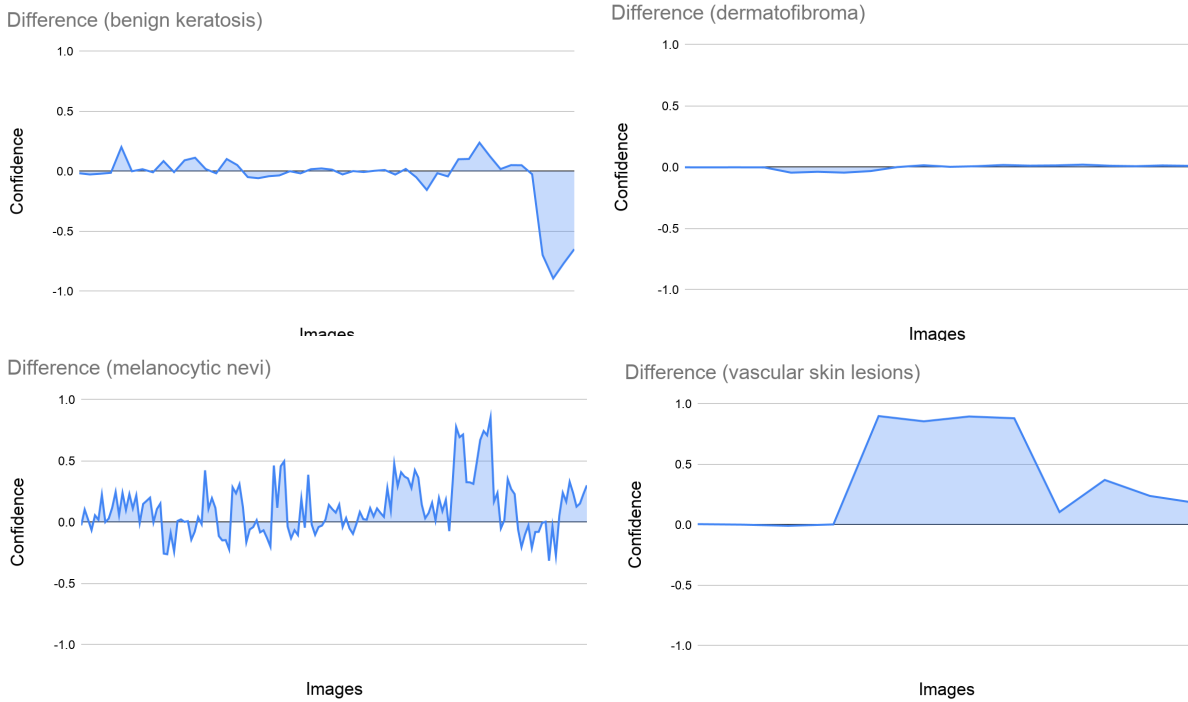


Figure 3. The differences between the confidence levels for polarized and non-polarized images for individual lesions were mapped in four more graphs, each graph for the four types of lesions. A positive value means that the confidence for a polarized image was higher than the non-polarized image. A negative value means the confidence for a non-polarized image was higher than the polarized image.

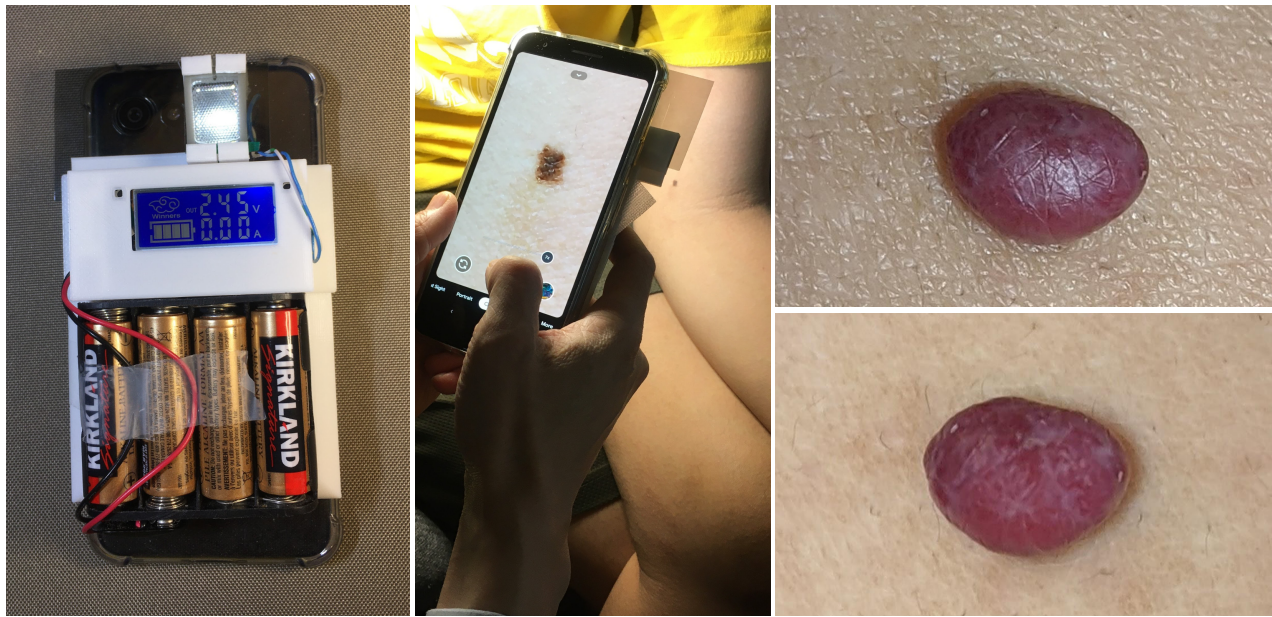


Figure 4. The *Polarizer Device* (leftmost image) and a demonstration of its use on a subject (middle image). Polarization of a vascular skin lesion shows visible reduction in glare and the revelation of some white subsurface structures (top rightmost image is non-polarized, bottom rightmost image is polarized).

Acknowledgements

I would like to thank my science teacher, Mr. Henri van Bommel, my adult sponsor, who guided me through the project and the application process.

References

- Rogers, H. W., Weinstock, M. A., Feldman, S. R., & Coldiron, B. M. (2015). Incidence Estimate of Nonmelanoma Skin Cancer (Keratinocyte Carcinomas) in the US Population, 2012. *JAMA Dermatology*, *151*(10), 1081. doi: 10.1001/jamadermatol.2015.1187
- Tannous, Z., Al-Arashi, M., Shah, S., & Yaroslavsky, A. N. (2009). Delineating melanoma using multimodal polarized light imaging. *Lasers in Surgery and Medicine*, *41*(1), 10–16. doi: 10.1002/lsm.20736
- Apalla, Z., Nashan, D., Weller, R. B., & Castellsagué, X. (2017). Skin Cancer: Epidemiology, Disease Burden, Pathophysiology, Diagnosis, and Therapeutic Approaches. *Dermatology and therapy*, *7*(Suppl 1), 5–19. doi:10.1007/s13555-016-0165-y
- European Society for Medical Oncology. (2018, May 28). *Man Against Machine: Artificial Intelligence is Better than Dermatologists at Diagnosing Skin Cancer [Annals of Oncology Press Release]*. Retrieved December 9, 2019, from <https://www.esmo.org/Press-Office/Press-Releases/Artificial-Intelligence-Skin-Cancer-Diagnosis>.
- American Academy of Dermatology. (2019, March 1). *Artificial intelligence shows promise for skin cancer detection*. Retrieved December 9, 2019, from <https://www.aad.org/news/ai-and-skin-cancer-detection>.
- Freeman, K., Dinnes, J., Chuchu, N., Takwoingi, Y., Bayliss, S. E., Matin, R. N., ... Williams, H. C. (2020). Algorithm based smartphone apps to assess risk of skin cancer in adults: systematic review of diagnostic accuracy studies. *Bmj*. doi: 10.1136/bmj.m645
- Esteva, A., Kuprel, B., Novoa, R. A., Ko, J., Swetter, S. M., Blau, H. M., & Thrun, S. (2017). Erratum: Corrigendum: Dermatologist-level classification of skin cancer with deep neural networks. *Nature*, *546*(7660), 686–686. doi: 10.1038/nature22985
- Louie, D. C., Phillips, J., Tchivaleva, L., Kalia, S., Lui, H., Wang, W., & Lee, T. K. (2018). Degree of optical polarization as a tool for detecting melanoma: proof of principle. *Journal of Biomedical Optics*, *23*(12). doi: 10.1117/1.JBO.23.12.125004
- Dimitriou, F., Scope, A., Braun, R. P., Reiter, O., & Marghoob, A. A. (2019). Polarized dermoscopy. *dermoscopedia*. Retrieved 03:03, December 9, 2019 from https://dermoscopedia.org/w/index.php?title=Polarized_dermoscopy&oldid=15355.
- Pan, Y., Gareau, DS., Scope, A., Rajadhyaksha M., Mullani NA., Marghoob AA.. Polarized and Nonpolarized Dermoscopy: The Explanation for the Observed Differences. *Arch Dermatol*. 2008;144(6):828–829. doi:10.1001/archderm.144.6.828
- Rosendahl, C., & Marozava, A. (2019). *Dermatoscopy and skin cancer: a handbook for hunters of skin cancer and melanoma*. Banbury: Scion Publishing Limited.
- Cohen YK, Elpern DJ, Wolpowitz D, Rosendahl C. Glowing in the dark: case report of a clue-poor melanoma unmasked by polarized dermatoscopy. *Dermatol Pract Concept*. 2014;4(1):83–87. Published 2014 Jan 31. doi:10.5826/dpc.0401a14
- Tschandl, P., Rosendahl, C. & Kittler, H. (2018). The HAM10000 dataset, a large collection of multi-source dermatoscopic images of common pigmented skin lesions. *Sci Data* *5*, 180161 (2018) doi:10.1038/sdata.2018.161

- Canadian Cancer Society. (n.d.). *Finding skin cancer early*. Retrieved December 9, 2019, from <https://www.cancer.ca/en/cancer-information/cancer-type/skin-melanoma/finding-cancer-early/?region=bc>.
- Kingma, D. I. P., & Ba, J. (2014). Adam: A Method for Stochastic Optimization. *Adam: A Method for Stochastic Optimization*. Retrieved from <https://arxiv.org/abs/1412.6980>

Bibliography

- Two-step algorithm. (2019, May 22). *dermoscopia*. Retrieved 01:51, February 16, 2020 from https://dermoscopia.org/w/index.php?title=Two-step_algorithm&oldid=15900.
- Tschandl, P. (2018). The HAM10000 dataset, a large collection of multi-source dermatoscopic images of common pigmented skin lesions. doi: 10.7910
- Cohen, Y., Elpern, D., Wolpowitz, D., & Rosendahl, C. (2014). Glowing in the dark: case report of a clue-poor melanoma unmasked by polarized dermatoscopy. *Dermatology Practical & Conceptual*. doi: 10.5826/dpc.0401a14
- Singh, P., & Manure, A. (2019). Neural Networks and Deep Learning with TensorFlow. *Learn TensorFlow 2.0*, 53–74. doi: 10.1007/978-1-4842-5558-2_3